Biomaterials and Biomedical Engineering, *Vol. 1, No. 1 (2014) 41-50*
DOI: http://dx.doi.org/10.12989/bme.2014.1.1.041

The *in vivo* photothermal treatment of gold nanorod in the mouse ear model

Bruce Yao Wen Liu[1,2], Cheng-Lung Chen[*1], Shin-Yu Lee[1], Fu-Hsiung Chang[3], Win-Li Lin[4], Chih-Ta Chia[2] and Yang-Yuan Chen[**1,5]

[1]*Institute of Physics, Academia Sinica, Taipei, Taiwan.*
[2]*Department of Physics, National Taiwan Normal University, Taipei, Taiwan*
[3]*Institute of Biochemistry and Molecular Biology, National Taiwan University, Taipei, Taiwan*
[4]*Institute of Biomedical Engineering, National Taiwan University, Taipei, Taiwan*
[5]*Graduate Institute of Applied Physics, National Chengchi University, Taipei, Taiwan*

(Received January 17, 2014, Revised March 18, 2014, Accepted March 18, 2014)

Abstract. Gold nanorod's exceptional light to heat transduction is a robust phonomenon that has been extensively verified. The phenomenon is a trait from which many novel applications across disciplines have been proposed. In this investigation, the feasibility of utilizing heat harvested from such photothermal method to combat cancer is presented. Using non-invasive laser methods, an *in vivo* study is conducted on mouse ear tumors administered with gold nanorods (Au NRs). An emphasis is placed on monitoring the tumor developments after photothermal treatments, over time. The findings reveal significant tumor growth surpression at a threshold laser power of 0.6 W/cm^2 lasting 2 minutes; this energy also brought about dramatic size reduction in treated tumors. Furthermore, the apparent formation of an eschar over the laser treated region indicates extensive hemorrhagic necrosis of the tumor tissue; a phenomenon implicative to the inhibition of angiogenesis.

Keywords: gold nanorod; photothermal; tumor; laser; cancer; necrosis

1. Introduction

Nano photothermal cancer therapeutics, the novel practice of heat treating malignant tumors using energy harvested from light activated nanomaterials, have received considerable interest for a while now; the method is advocated as, at the least, a strategically beneficial candidate for the next generation of cancer treatments (Menon *et al.* 2013). Au NRs in particular, with its biocompatibility and fascinating optical properties, have been adopted extensively in photothermal therapeutic studies (Ekici *et al.* 2008). However, further studies beyond petri dishes—i.e., studies that clinical or posing *in vivo* relevance at the least—are rather limited. Specifically, investigations into the variation in tumor sizes and their corresponding pathological characteristics subsequent to photothermal treatment should prove to be insightful. For *in vivo* studies that have been reported

∗Corresponding author, Ph.D., E-mail: aabbss@phys.sinica.edu.tw
**Ph.D., E-mail: cheny2@phys.sinica.edu.tw

Copyright © 2014 Techno-Press, Ltd.
http://www.techno-press.org/?journal=bme&subpage=7 ISSN: 2288-3738 (Print), 2288-3746 (Online)

(Dickerson *et al.* 2008), despite the comprehensive pathological characterisation, vascular variation beneath the tissue proved difficult to monitor: a drawback due to the preference towards the back or rear flank areas of the mice to study. Angiogenesis has recently been suggested as critical for the growth of primary tumors and the onset of metastasis. However, studies on the vasculature variation after therapy are rather limited (Zetter 1998). Indeed, tumor vasculature shutdown, and further induced anti-tumor immune response are, today, some of the most promising strategies in restricting tumor growth (Chen *et al.* 2006). Therefore, in terms of photothermal treatment, more emphasis should be placed on revealing the influence of post-therapy vascular development, and the structural variation of surrounding tissue after tumor destruction.

To resolve previously mentioned drawbacks, our investigation opted for the mouse ear as the model system instead. This is by virtue of its extremely thin structure, making the mouse ear the perfect model system in studying variations in tumor microenvironment, and the angiogenic activity of tumors (Pourtier-Manzanedo *et al.* 2003). As for the photothermal agent, Au NRs, an optimum dimension is first determined from two samples produced by different methods. Specifically, their photothemolysis efficacies in an *in vitro* setting were compared. The smaller of the two groups exhibited superior photothermal properties, and were thus employed in the subsequent mouse ear tumor phtothermal studies to clarify the tumor vascular vessel variations and tumor size developments (Lin *et al.* 2012). The observations presented hereafter demonstrate the merit of mouse ear models in understanding the primary mechanism of *in vivo* photothermal tumor treatment, and further supports the feasibility of Au NRs in clinical phototherapeutic applications.

2. Materials & methods

2.1 Preparation of gold nanorods

Au NRs were synthesized from two methods: the seeding growth method (Nikoobakht and El-Sayed 2003) and the seedless-growth method (Jana 2005). The Au NRs were characterized using UV-visible absorption spectrum and transmission electron microscopy (TEM). To attain biocompatibility, the surface of Au NRs was further modified with polystyrenesulfonate (PSS-Au NRs). The aliquots of Au NRs were also subjected to inductively coupled plasma mass spectroscopy (Thermo, Xseries 2) to correlate optical density (O.D.) with weigh concentration. Comparison against a calibration line showed a gold content of ~22 μg/mL at O.D.1.

2.2 Cell line

The EMT-6 cell is a transplantable murine mammary tumor cell line that has been served as a model to study the effects of various treatments on local tumor growth and pulmonary metastasis. The cell cultures were maintained in a humidified atmosphere containing 5% CO_2 at 37^{o}C. The medium involved 1% penicillin-streptomycin (Invitrogen) and 10% fetal bovine serum (FBS, Invitrogen). The number of cells was counted using a hemocytometer.

2.3 In vitro cancer cell photothermolysis

In vitro photothermolysis was carried out on an inverted scanning microscope (LSM510, META/Observer, Z1, Zeiss). A femtosecond (fs) Ti:Sapphire laser (Spectra-physics MaiTai HP) with a duration time of 100 fs and a repetition rate of 80 MHz was used as the excitation source. The wavelength and average power of the laser beam were both tunable, and a water-immersion objective lens (NA=1.4) was used. To effectively excite Au NRs, the laser wavelength was tuned to 800 nm. Typically, an area of 90 μm × 90 μm (512 pixels × 512 pixels) was scanned at a rate of 1.57 s for imaging, and thereby the exposure time per pixel per scan is 5.98 μs (each pixel area=176×176 nm^2). For cancer cell photothermolysis mediated by AuNRs, a relatively slow exposure time of 164 μs per pixel per scan was applied to activate the Au NRs. The detailed calculations of deposited energy fluences upon AuNRs can be obtained from the literature (Tong *et al.* 2007). In this work, one scan of threshold excited power density (~12 W/cm^2) was applied to the specimens. The corresponding energy fluence is calculated to be ~6 mJ/cm^2.

2.4 Tumor inoculation & Au NR injection

Female Balb/c mice, 4-6 weeks of ages, were obtained from BioLASCO Taiwan Co., Ltd and handled in accordance with the guidelines of the Institution of Animal Care and Use Committee of National Taiwan University in Taiwan. To induce solid tumors in the mouse ear, the suspended EMT-6 cells (~10^6 cells in 30 μL medium) were injected subcutaneously into both ears of the mouse. Considering the preferred route of Au NR administration in photothermal cancer therapy reported by Huang *et al.* (2010), the nanorods (~10 μg) were intratumorally injected into the tumor (~30 mm^3). The related controls were also treated accordingly. No adverse effects were observed in tumor growth from the administration of Au NRs; this suggests its feasibility for further studies in *in vivo* photothermal therapeutics. The morphology and area of the tumors were analyzed by using the stereo microscope, Leica MZ16FA, and the thickness was measured by a vernier. Therefore, the tumor volume was calculated using the following equation: tumor volume (mm^3) = $\pi/6$ × area (mm^2) × t (mm), where t is the thickness of solid tumor. Data were analyzed using the VassarStats Online Calculator (http://vassarstats.net/). The significance level for the differences between groups (p-value) was determined using the one way ANOVA Tukey HSD Test. p-value < 0.05 was considered to be statistically significant.

2.5 In vivo photothermal treatments on the tumor

Pulse lasers, as utilized in *in vitro* systems described previously, are capable of transiently inducing microbubbles around overheated optical absorbers. In contrast, continuous wave (CW) lasers have lower photon absorption efficiency and therefore requiring comparatively longer exposure time to heat and destroy the target through thermal protein denaturation. Nevertheless, the latter is more suited to treating tumors of larger size, and thus our preference of it as the excitation source for the *in vivo* studies. In this study, the ears of the mice were irradiated with a CW near infrared (NIR) laser (808 nm diode laser) to the tumor region. Burn scarring of the ear skin was avoided by restricting the laser doses to within 0.8 W/cm^2 times 2 minutes.

A representation of the *in vivo* photothermal procedure is shown in Fig. 1. 12 days after the EMT-6 tumor cells were homografted on mice ears, the tumor sizes grew to approximately 30

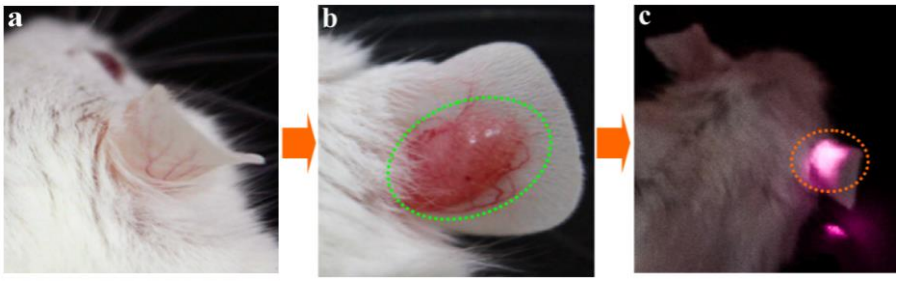

Fig. 1 *In vivo* photothermal treatments using Au NRs. (a) without any tumor on the ear; (b) the mouse ear bearing EMT-6 breast tumor; (c) the mouse ear tumor subjected to the photothermal treatment

mm^3 in size, (Fig 1(b)), and were then intratumorally injected with Au NRs. After 24 h, the mouse ear was irradiated with a CW laser at a power density of 0.6 W/cm^2 for 2 min (Fig 1(c)). The tumor development was then continuously monitored under a stereo microscope thereafter. The data presented in this article was concluded from four independent experiments with similar procedures.

2.6 Histology study

After the mice were euthanized by cervical dislocation, the tissues of interest were resected and processed by the following histological section steps: gross cutting, fixation, microtome cutting and mounting. The excised tumor tissue was embedded in paraffin blocks, sectioned into 5-10 mm slices, and stained with hematoxylin/ eosin (H&E) to study the tissue and cellular morphology. The histology images were viewed and acquired with a Leica DMIRB microscope (Leica Microsystems).

3. Results and discussion

3.1 Characterization of gold nanorods

The Au NRs used in this study are synthesized from two methods described below: the seedless-growth of Au NRs and the seed-mediated growth of Au NRs. Compared with the seed-mediated growth of Au NRs, the seedless growth of Au NRs is a more simplistic method in producing Au NR in large quantities. The particle size (length × width) obtained by seedless -growth is around 27 nm × 7 nm, and that by seed-mediated growth is around 40 × 10 nm (Fig. 2(a)-(b)); the aspect ratio of the nanorods in both methods can be readily controlled to ~3.9. Furthermore, the corresponding longitudinal surface plasmon absorption peak is nearly the same as Au NRs prepared by the seed-mediated growth method reported by Chen *et al.* (2010) (Fig. 2(c)).

For the purpose of biocompatibility, the surfaces of Au NRs were further modified with polystyrenesulfonate sodium salt (PSS, 70 kDa). After introducing Au NRs into cellular environment, most of the ingested Au NRs were found to gather into numerous clusters in several vesicular structures. The *in vitro* photothermolysis of 27 and 40 nm Au NRs were compared by monitoring their simultaneous transition of cellular nucleus using the fluorescent dye exclusion

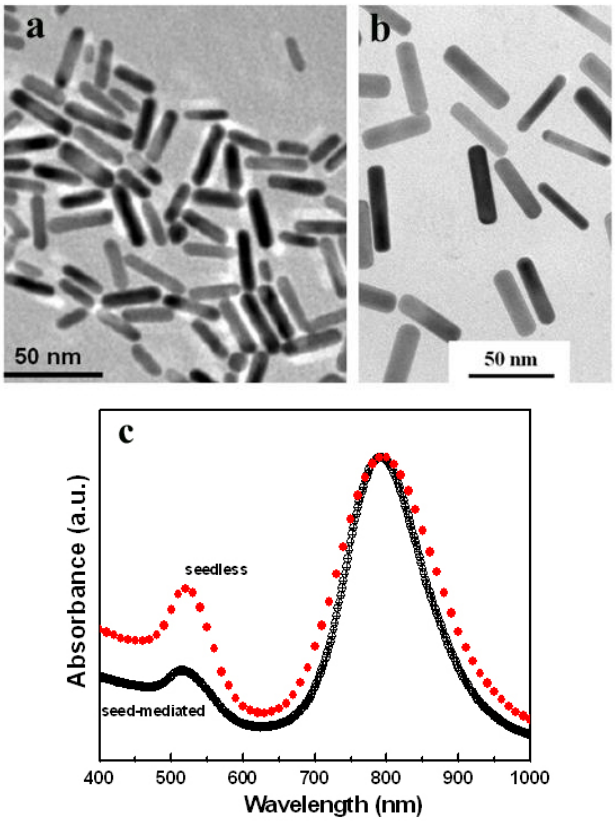

Fig. 2 TEM images of Au NRs obtained by the seedless (a) and seed-mediated growth methods (b). (c) Absorption spectra of Au NRs

method (Chen *et al.* 2010). This technique entails the application of two dyes, YOPRO-1 (green coloring) and propidium iodide (red coloring), to qualitatively monitor plasma membrane integrity of the cells as an indication of cell viability. Separate controls of EMT-6 cancer cells without Au NRs were subjected to laser irradiation, wherein uninjurious laser energy thresholds were determined. It is found that, typically, a relatively lower population of ingested 27 nm nanorods (based on the confocal laser scanning microscopic images) is sufficient in reducing the laser energy fluence threshold for effectively destroying cancer cells by about 2~3 times lower when compared to 40 nm Au NRs prepared by the seeding method (Chen *et al.* 2010) (Fig. 3). The differences can be explained by the following reasons. First, it is understood, in light of energy transduction, that high optical absorption efficiency of nanorods is essential for effective photothermal therapy. The surface plasmon resonance of Au NRs enhances not only the absorption but also the scattering; the relative contribution of each towards the total optical extinction, depends on the nanorods size and aspect ratio. Based on the theoretical calculations proposed by Lee and El-Sayed (2005), plasmonic absorption has a dominant effect for smaller Au NRs, and scattering is dominant for larger ones. Thus, being three times smaller than those prepared by the seed-mediated growth method, Au NRs grown by the seedless growth method therefore exhibits greater plasmonic absorption. The conclusion could also be understood from the optical absorption

results reported by Ali *et al*. (2012). As relatively smaller Au NRs can be uniformly distributed to a larger area in smaller numbers (Fig. 3(a)), a smaller energy output is needed for activating these widespread nanorod clusters to reach microbubble-formation thresholds during laser illumination (Zharov *et al*. 2005). Not only does this play a crucial role in selective photothermolysis of cancer cells targeted with nanorods, but it also assists in developing larger numbers of perforations within the cellular membrane. In accordance with the results, the one-pot seedlessly synthesized Au NRs were selected as the photothermal agent for the *in vivo* cancer treatment.

3.2 In vivo photothermal treatments

As expected, these Au NRs assisted with NIR excitation remarkably suppressed tumor growth compared to the other three control groups (Untreated tumor, phosphate buffered salin (PBS) + NIR, and AuNRs only), and showed complete destruction of the tumor by the 16th day after the treatment (Fig. 4). Moreover, a significant change in the tumor vasculature, caused by vascular bed shrink and collapse, was observed (Fig. 5). The consequent inhibition of angiogenesis may further contribute to the suppression of tumor growth. The treated mice were able to survive at least the 3-month post-observation period. Contrasting this, tumors treated in the control groups continued to proliferate, eventually leading to the death of the mice. These results demonstrate the efficacy and feasibility of Au NRs photothermal treatment *in vivo*. It is worth noting that tissue eschar

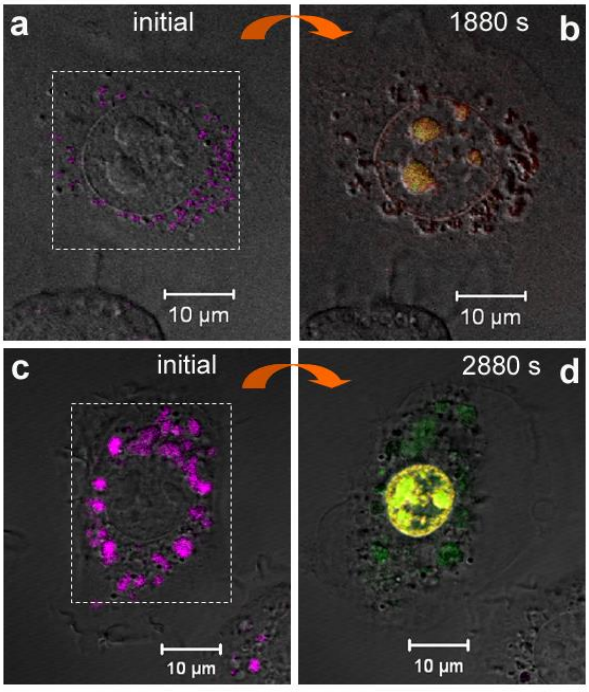

Fig. 3 Photothermolysis of the EMT-6 tumor cell triggered by two kinds of Au NRs. The laser activation area is marked with dash line, and the pink spots are the locations of Au NR clusters. (a)-(b) the threshold laser energy fluences of seedless grown Au NRs is ~ 6 mJ/cm^2; (c)-(d) the threshold laser energy fluences of seed-mediated grown Au NRs is ~18 mJ/cm^2 (Chen *et al*. 2010)

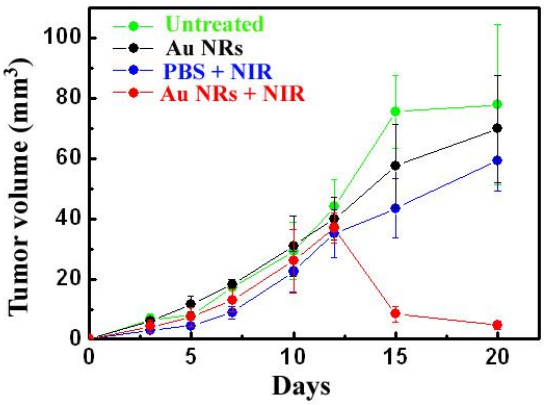

Fig. 4 Time-dependent tumor growth curves of EMT-6 tumor cell homografts. Four conditions were studied: untreated control (group 1), Au NRs (group 2), PBS plus NIR laser (group 3), and Au NRs plus NIR laser (group 4). The sample treatments were conducted at the 12th day, and the results were shown as the arithmetic means of tumor volumes in each group (n = 3). Only the Au NRs + NIR treated group presents significant tumor regression compared with other experimental groups, $P < 0.05$ for group 1 to 3 versus group 4

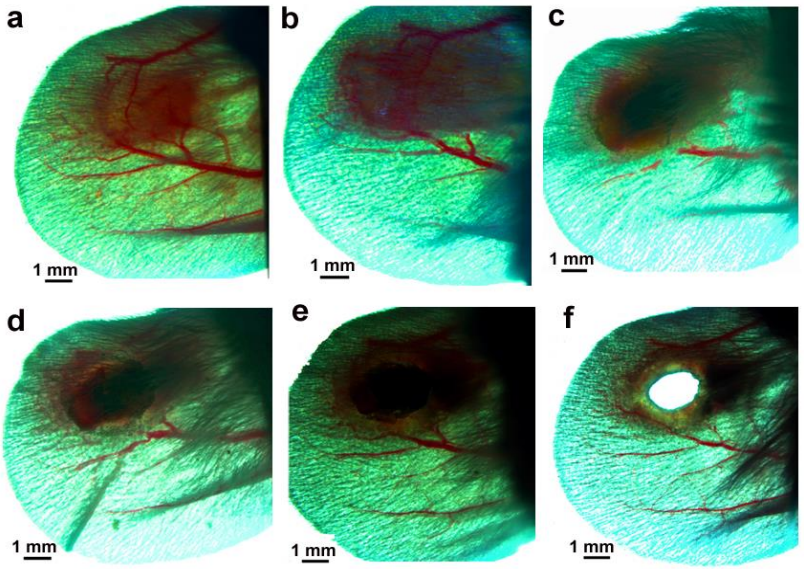

Fig. 5 Photomicrographs of mouse-ear tumor development before and after the treatment of Au NRs + NIR irradiation with 0.6 W/cm^2 for 2 min: (a)3, (b)11, (c)18, (d)21, (e)27, (f)39 days. The tumor was treated at the 12th day. The result shows that an eschar was clearly observed on the 21th day, and eventually became a hollow structure on the ear on the 39th day

appeared over the laser treated region on the 9th day after the treatment, which leads on to form a hollow structure on the ear. This is a direct evidence of the generation of excessive local heat from laser excited Au NRs, and indicates massive hemorrhagic necrosis of the tumor (Nishimura *et al.*

1988). In general, the eschar of the wound falls off a few days later, revealing normal healthy tissue. Nevertheless, the ear structure is probably too thin to reconstruct from such trauma. Attempts in reducing the power density to 0.5 W/cm^2, were unable to destroy the primary tumor completely, and the mice died due to metastasis of the primary tumor (Hoshida *et al.* 2006).

3.3 Histological examination

We further examined the histological section of tumor tissues that were treated with Au NRs + NIR irradiation. For this purpose, two groups of mice were sacrificed at different time points, and their corresponding H&E staining of post-treatments were observed. During the early stage, the appearance of the tumors did not show any obvious variation, whereas, later, a substantial vacant space formed in the central part of the tumor tissue due to the eradication of a large number of tumor cells (Fig. 6(a)). As for the other group of tumor tissue that was histologically sectioned on the 8th day after the treatment, we found the tumor tissue eventually developed into an eschar, and showed an absence of residual tumor cells in the photothermally treated region (Fig. 6(b)). According to these histological results, we speculate that the tumor tissue may undergo the following process during local acute hyperthermia excitation (Nishimura *et al.* 1988): a marked dilatation and congestion of the vascular vessels surrounding the tumor tissue occurrs at initial heating stage (~ 41^{o}C). Further petechiation, stasis, and thrombosis form at a relatively higher temperature (~ 43^{o}C). Once the temperature reaches ~ 45^{o}C, recanalization of the tumor vessels shuts down, and brings about a massive hemorrhage due to the rupturing of tumor vessel walls. Hypoxia, in conjunction with an imbalance of pH and energy supply of the cell, will also cause tumor cell necrosis, and facilitate tumor size suppression (Pelz *et al.* 2004). Although much work is needed to systematically study these complicated Au NR-mediated hyperthermia processes, our investigations well demonstrate the excellent destructive effects of photo-excited Au NRs on tumor microvascular architecture and functions.

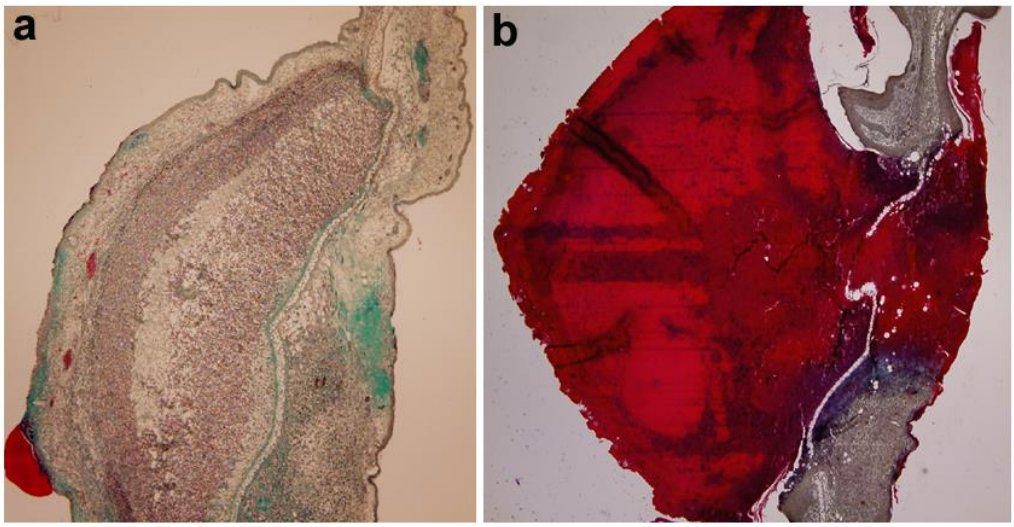

Fig. 6 Representative histological section images of EMT-6 tumor tissues that were treated with Au NRs and NIR irradiation from the two mice ears after different time points of treatments: (a) 1day, (b) 8days

4. Conclusions

The small-sized Au NRs proved to be excellent photothermal agents in photothermal treatment *in vitro*, which was further demonstrated in solid tumors *in vivo*. When the tumor was treated with Au NRs + NIR, the excessive local heating generated from light activated Au NRs was sufficient to destroy the tumor. The generation of an eschar over the laser treated region represents massive hemorrhagic necrosis of the tumor tissue.

Acknowledgements

This work was supported by the National Science Council of the Republic of China under Grant No. NSC 100-2112-M-001-019-MY3. We thank Prof. Yeu-Kuang Hwu and Prof. Chi-Keung Chan for the experimental help, and Mr. Cheng-Kuang Huang for his constructive discussion.

References

Ali, M.R.K., Snyder, B. and El-Sayed, M.A. (2012), "Synthesis and optical properties of small Au nanorods using a seedless growth technique", *Langmuir*, **28**(25), 9807-9815.

Chen, X.Y., Zhang, W. and Zhang, W. (2006), "Vaccination with viable human umbilical vein endothelial cells prevents metastatic tumors by attack on tumor vasculature with both cellular and humoral immunity", *Clin. Cancer. Res.*, **12**(19), 5834-5840.

Chen, C.L., Kuo, L.R. and Chang, C.L. (2010), "In situ real-time investigation of cancer cell photothermolysis mediated by excited gold nanorod surface plasmons", *Biomaterials*, **31**(14), 4104-4112.

Dickerson, E.B., Dreaden, E.C. and Huang, X.H. (2008), "Gold nanorod assisted near-infrared plasmonic photothermal therapy (PPTT) of squamous cell carcinoma in mice", *Cancer. Lett.*, **269**(1), 57-66.

Ekici, O., Harrison, R.K. and Durr, N.J. (2008), "Thermal analysis of gold nanorods heated with femtosecond laser pulses", *J. Phys. D. Appl. Phys.*, **41**(18), 185501-185511.

Hoshida, T., Isaka, N. and Hagendoorn, J. (2006), "Imaging steps of lymphatic metastasis reveals that vascular endothelial growth factor-C increases metastasis by increasing delivery of cancer cells to lymph nodes: Therapeutic implications", *Cancer. Res.*, **66**(16), 8065-8075.

Huang, X.H., Peng, X.H. and Wang, Y.Q. (2010), "A reexamination of active and passive tumor targeting by using rod-shaped gold nanocrystals and covalently conjugated peptide ligands", *Acs. Nano.*, **4**(10), 5887-5896.

Jana, N.R. (2005), "Gram-scale synthesis of soluble, near-monodisperse gold nanorods and other anisotropic nanoparticles", *Small*, **1**(8-9), 875-882.

Lee, K.S. and El-Sayed, M.A. (2005), "Dependence of the enhanced optical scattering efficiency relative to that of absorption for gold metal nanorods on aspect ratio, size, end-cap shape, and medium refractive index", *J. Phys. Chem. B.*, **109**(43), 20331-20338.

Lin, C.Y., Tseng, H.C. and Shiu, H.R. (2012), "Ultrasound sonication with microbubbles disrupts blood vessels and enhances tumor treatments of anticancer nanodrug", *Nanomedicine-UK*, **7**(1), 2143-2152.

Menon, J.U., Jadeja, P. and Tambe, P. (2013), "Nanomaterials for photo-based diagnostic and therapeutic applications", *Theranostics*, **3**(3), 152-166.

Nishimura, Y., Hiraoka, M. and Jo, S. (1988), "Microangiographic and histologic analysis of the effects of hyperthermia on murine tumor vasculature", *Int. J. Radiat. Oncol.*, **15**(2), 411-420.

Nikoobakht, B. and El-Sayed, M.A. (2003), "Preparation and growth mechanism of gold nanorods (NRs) using seed-mediated growth method", *Chem. Mater.*, **15**(10), 1957-1962.

Pourtier-Manzanedo, A., Vercamer, C. and Van-Belle E. (2003), "Expression of an Ets-1 dominant-negative mutant perturbs normal and tumor angiogenesis in a mouse ear model", *Oncogene*, **22**(12), 1795-1806.

Pelz, J., Mollwitz, M. and Stremmel, C. (2004), "The impact of surgery and mild hyperthermia on tumor response and angioneogenesis of malignant melanoma in a rat perfusion model", *Bmc. Cancer.*, **4**(52), 1-9.

Tong, L., Zhao, Y. and Huff, T.B. (2007), "Gold nanorods mediate tumor cell death by compromising membrane integrity", *Adv. Mater.*, **19**(20), 3136-3141.

Zetter, B.R. (1998), "Angiogenesis and tumor metastasis", *Annu. Rev. Med*., **49**(1), 407-424.

Zharov, V.P., Galitovskaya, E.N. and Johnson, C. (2005), "Synergistic enhancement of selective nanophotothermolysis with gold nanoclusters: potential for cancer therapy", *Laser. Surg. Med*., **37**(3), 219-226.

YC